



Published in final edited form as:

*Magn Reson Med.* 2015 December ; 74(6): 1632–1639. doi:10.1002/mrm.25575.

## Combined Outer Volume Suppression and $T_2$ Preparation Sequence for Coronary Angiography

Jieying Luo<sup>1</sup>, Nii Okai Addy<sup>1</sup>, R. Reeve Ingle<sup>1</sup>, Brian A. Hargreaves<sup>2</sup>, Bob S. Hu<sup>1,3</sup>, Dwight G. Nishimura<sup>1</sup>, and Taehoon Shin<sup>4</sup>

<sup>1</sup>Department of Electrical Engineering, Magnetic Resonance Systems Research Laboratory, Stanford University, Stanford, California, USA

<sup>2</sup>Department of Radiology, Stanford University, Stanford, California, USA

<sup>3</sup>Palo Alto Medical Foundation, Palo Alto, California, USA

<sup>4</sup>Diagnostic Radiology and Nuclear Medicine, University of Maryland, Baltimore, Maryland, USA

### Abstract

**Purpose**—To develop a magnetization preparation sequence for simultaneous outer volume suppression (OVS) and  $T_2$  weighting in whole-heart coronary magnetic resonance angiography (MRA).

**Methods**—A combined OVS and  $T_2$  preparation sequence (OVS- $T_2$  Prep) was designed with a nonselective adiabatic  $90^\circ$  tipdown pulse, two adiabatic  $180^\circ$  refocusing pulses, and a 2D spiral  $-90^\circ$  tipup pulse. The OVS- $T_2$  Prep preserves the magnetization inside an elliptic cylinder with  $T_2$  weighting, while saturating the magnetization outside the cylinder. Its performance was tested on phantoms and on thirteen normal subjects with coronary MRA using 3D cones trajectories.

**Results**—Phantom studies showed expected  $T_2$ -dependent signal amplitude in the spatial passband and suppressed signal in the spatial stopband. In vivo studies with full-FOV cones yielded a passband-to-stopband signal ratio of  $3.18 \pm 0.77$  and blood-myocardium contrast-to-noise ratio enhancement by a factor of  $1.43 \pm 0.20$  ( $P < 0.001$ ). In vivo studies with reduced-FOV cones showed that OVS- $T_2$  Prep well suppressed the aliasing artifacts, as supported by significantly reduced signal in the regions with no tissues compared to the images acquired without preparation ( $P < 0.0001$ ).

**Conclusion**—OVS- $T_2$  Prep is a compact sequence that can accelerate coronary MRA by suppressing signals from tissues surrounding the heart while simultaneously enhancing the blood-myocardium contrast.

### Keywords

outer volume suppression;  $T_2$  Prep; cones imaging; RF pulse design; coronary MR angiography

## Introduction

Three-dimensional whole-heart coronary magnetic resonance angiography (MRA) has long been sought as an alternative to X-ray angiography due to its noninvasive and non-ionizing nature and flexibility of post-analysis through arbitrary views. However, robust visualization of the coronary arteries remains challenging due to several technical requirements, including high spatial resolution and vessel contrast, and immunity to cardiac and respiratory motion. A long scan time is one of the challenging outcomes of such requirements. Due to the large size of data to be acquired as well as low acquisition efficiencies caused by cardiac and respiratory gating, the total scan time easily exceeds 9 min for typical imaging parameters (1, 2).

Parallel imaging is the method of choice for scan acceleration with the widest availability on clinical scanners. Although its performance has been well demonstrated at relatively low acceleration factors (2–4) (3, 4), higher acceleration suffers from loss in the signal-to-noise ratio (SNR) (5). Compressed sensing has recently been applied to high-rate scan acceleration and shown to yield superior performance over parallel imaging, but at the cost of substantial increase in reconstruction time and complexity (6). Time-efficient non-Cartesian k-space acquisition is another approach for scan acceleration with an additional benefit of benign motion and flow properties (7, 8). Recently, 3D cones trajectories combined with 2D spiral navigators have shown great promise for coronary MRA in healthy and patient subjects, allowing isotropic spatial resolution and 100% acquisition efficiency (9, 10).

In this work, we propose a new magnetization preparation sequence for coronary MRA which combines outer volume suppression (OVS) (11–14) with  $T_2$  preparation (15–17). This preparation sequence saturates signals outside a 2D region of interest (ROI), thus reducing the required imaging field-of-view (FOV) and enabling scan time reduction. This sequence also simultaneously generates  $T_2$  contrast that is routinely used for improving blood-myocardium contrast in coronary MRA. The performance of the proposed OVS- $T_2$  prep sequence is demonstrated on phantoms and in vivo with coronary MRA protocols with full-FOV and reduced-FOV 3D cones trajectories (9).

## Methods

### Sequence design

The design parameters of the proposed OVS- $T_2$  Prep pulse sequence are optimized for imaging at 1.5 T. Figure 1 shows the timing diagram of the OVS- $T_2$  Prep sequence. A nonselective  $90^\circ$  adiabatic pulse (BIR-4) (18) is first applied, tipping down all longitudinal magnetization into the transverse plane. After the tipdown pulse, the transverse magnetization experiences  $T_2$  decay during a  $T_2$  Prep time (TE). Two identical  $180^\circ$  adiabatic full passage (AFP) pulses (19–21) are applied at TE/4 and 3TE/4 after the tipdown pulse to refocus the dephasing caused by off-resonance. These two AFP pulses also prevent  $T_1$  recovery of tissues in the spatial stopband during TE due to the double inversion recovery effect (22). At TE after the tipdown pulse, a 2D  $-90^\circ$  spiral RF pulse restores the  $T_2$ -weighted magnetization within an elliptical region back to the longitudinal direction. Each of the two elliptical axes can be resized by scaling the X and Y gradients of the spiral pulse

independently. This feature enables easy customization of the size of the in-plane spatial passband over subjects. The transverse magnetization outside the passband is dephased by the gradient spoilers applied along all three gradient axes at the end of the sequence ( $G_z$  is not shown in Fig. 1).

For robustness to  $B_0$  and  $B_1$  inhomogeneities at 1.5 T, the design parameters of BIR-4 and AFP were chosen as follows. The peak RF amplitude of the sequence is set to 0.18 G. The BIR-4 pulse is designed with a hyperbolic tangent amplitude of  $\beta = 10$  and a tangent frequency modulation of  $\tan(\lambda) = 50$ . The AFP is designed with a hyperbolic secant amplitude and hyperbolic tangent phase modulation ( $\mu = 2.5$ ,  $\beta = 980$ ). With these design parameters, simulation shows that the phase dispersion angle at the end of the preparation sequence is less than  $23.8^\circ$  within the off-resonance range of  $[-100, +100]$  Hz and  $B_1$  scale range of  $[80\%, 120\%]$  (defined as actual  $B_1$ /nominal  $B_1$ ).

The  $-90^\circ$  2D tipup pulse was designed using a single-shot spiral excitation k-space trajectory. A unique feature of this 2D tipup is that its spatial profile is a combination of the real and imaginary components of the conventional tipdown profiles where the imaginary component contains the excitation mainlobe and even-ordered sidelobes, and the real component contains the odd-ordered sidelobes (14). By tuning the phase difference between the spiral tipup pulse and the transverse magnetization at the echo of the second AFP, only the imaginary component of the profile returns to the longitudinal direction, which excludes the first sidelobe and therefore doubles the distance between the main and aliased excitations. This is equivalent to what would have been generally yielded with two interleaved spirals, and can be leveraged to reduce the duration of the spiral pulse. The design parameters of the spiral tipup pulse were an elliptical passband width of 12 cm in the anterior/posterior (A/P) direction and 16 cm in the left-right (L/R) direction, time-bandwidth product of 4.0, and two-sided stopband width of 24 cm in the A/P direction and 34 cm in the L/R direction. The resultant duration of the spiral gradient waveforms was 3.2 ms, relatively short helping to avoid the effects of off-resonance.

Bloch simulations of the OVS- $T_2$  Prep sequence were performed to evaluate resultant  $M_z$  profiles for arterial blood ( $T_1 = 1000$  ms,  $T_2 = 230$  ms), myocardium ( $T_1 = 870$  ms,  $T_2 = 50$  ms) and fat ( $T_1 = 230$  ms,  $T_2 = 85$  ms) at 1.5 T. The  $B_0$  and  $B_1$  field inhomogeneities were considered in the ranges of  $[-100, 100]$  Hz and  $[80\%, 120\%]$  of the nominal  $B_1$  value, respectively. The initial  $M_z/M_0$  was assumed to be 1 for arterial blood and myocardium, while it was assumed to be 0 for fat assuming spectrally selective fat saturation immediately before the OVS- $T_2$  Prep sequence.

## Imaging experiments

All experiments were conducted on a 1.5 T GE Signa Excite scanner with a maximum gradient amplitude of 40 mT/m and a maximum gradient slew rate of 150 mT/m/ms. The phantom studies used a birdcage head coil and the in vivo studies used an eight-channel cardiac coil for signal reception. This study was approved by the IRB, and written informed consents were obtained from all the participants.

To evaluate the performance of the OVS- $T_2$  Prep sequence, phantom experiments were done with a single-slice gradient-echo sequence (TR = 5 s, gradient echo time = 2.2 ms, flip angle =  $90^\circ$ ). A long TR and one view per preparation were used to accurately capture the longitudinal magnetization immediately after the preparation sequence without saturation effects. Three bottle-phantoms with  $T_1/T_2 = 1000$  ms/230 ms,  $T_1/T_2 = 250$  ms/50 ms and  $T_1/T_2 = 100$  ms/20 ms and one chicken muscle phantom with  $T_1/T_2 = 890$  ms/45 ms were scanned with and without preparation to demonstrate the OVS and  $T_2$  weighting performance.

In vivo experiments were performed to demonstrate the benefit of the proposed preparation sequence in coronary MRA. All in vivo scans used a free-breathing whole-heart technique based on the 3D cones trajectory and 2D image-based navigators (iNAV) (9). The MRA sequence diagram is shown in Fig. 2. In each heartbeat (R-R interval), a 2D iNAV was acquired and followed by a fat saturation module (F). Then the OVS- $T_2$  Prep sequence was applied immediately before the 3D cones image acquisition (IMG). A  $T_2$  Prep time of 20 ms was chosen to balance the blood-myocardium contrast enhancement with the signal loss of the blood. The size of the elliptical OVS passband was set to 12 cm (A/P)  $\times$  16 cm (L/R). For the 3D cones k-space acquisition, an alternating repetition time balanced steady-state free precession (ATR-SSFP) readout sequence was used for further suppression of fat signal (23). A second 2D iNAV was acquired after the 3D cones image acquisition. The two 2D iNAVs were acquired in the sagittal plane (tracking superior/inferior (S/I) and A/P motions) and the coronal plane (tracking S/I and L/R motions). A 3D translational motion model was obtained by combining the motion estimates from the two iNAVs. Linear phase compensation was applied in k-space accordingly for retrospective motion correction. The iNAVs were acquired using a 12 interleaved 2D spiral gradient-echo sequence with gradient echo time = 1.6 ms, TR = 6.3 ms, slice thickness = 8 mm, FOV = 28 cm, in-plane resolution = 3.1 mm, and acquisition duration = 76 ms. The imaging parameters for the coronary MRA sequence were gradient echo time = 0.57 ms, TR<sub>1</sub>/TR<sub>2</sub> = 4.29/1.15 ms, flip angle =  $70^\circ$ , receiver bandwidth =  $\pm 125$  kHz, views per segment = 18 (acquisition window = 98 ms), isotropic spatial resolution = 1.2 mm, and 100% respiratory navigator efficiency.

Coronary MRA with 3D cones was performed on thirteen healthy volunteers (eight males, age =  $28 \pm 4$ ). Three different cones trajectories were used with and without the OVS- $T_2$  Prep, yielding six data sets for each subject. The three trajectories were designed for in-plane FOVs of 28, 16 and 8 cm, respectively (hereafter termed FOV-28-Cones, FOV-16-Cones, and FOV-8-Cones). These trajectories have acquisition durations of 508 heartbeats, 289 heartbeats and 145 heartbeats respectively, corresponding to acceleration factors of 1, 1.8 and 3.5. An S/I FOV of 14 cm was used for all three trajectories. The trajectory design parameters are described in Table 1 along with the cross sections of the corresponding point spread functions. Like other center-out trajectories, 3D cones trajectories are oversampled near the k-space center; therefore, the achieved FOV can appear larger than the value prescribed in the design process, as demonstrated in the point spread functions (24, 25). All images were reconstructed at a 0.6 mm isotropic voxel size using two-fold interpolation by k-space zero-padding.

Quantitative analysis was performed with the following metrics. For the full-FOV scans, two metrics were defined to evaluate the outer volume suppression and the blood-myocardium contrast enhancement: (i) the passband-to-stopband signal ratio with preparation, defined as  $R_{PS} = S_{PASS,W}/S_{STOP,W}$ , where  $S_{PASS,W}$  and  $S_{STOP,W}$  are the average signals of ROIs in the muscle in the passband and stopband. These two ROIs were carefully selected such that the ratio of their mean signals without preparation was approximately 1. (ii) the ratio of contrast-to-noise ratio (CNR) with preparation to CNR without preparation, defined as  $R_C = CNR_W/CNR_{WO}$ ,  $CNR = (S_{LV} - S_{MYO})/\sigma_{LV}$ , where  $S_{LV}$  and  $\sigma_{LV}$  are the average and standard deviation of signal in an ROI of the left ventricle (LV) and  $S_{MYO}$  is the average signal of an ROI in the myocardium. For the reduced-FOV scans, the average signal in an ROI in the background where no tissue existed ( $S_{BKGD}$ ) was used as the metric for evaluating the aliasing artifacts (26). Paired two-tailed Student's *t*-tests were used to analyze the effect of the OVS- $T_2$  Prep on CNR and  $S_{BKGD}$ , with  $P < 0.05$  considered as statistically significant (27).

Qualitative image assessment was performed by two board-certified cardiologists. Per subject, thin-slab maximum intensity projection (MIP) reformats of LAD and RCA were generated from the images obtained with FOV-8-Cones and FOV-28-Cones using OsiriX (Pixmeo, Geneva, Switzerland). For each coronary territory and subject, the two images obtained with and without OVS- $T_2$  Prep were displayed as pairs side by side with randomized display positions. In total across 13 subjects, 52 images pairs were evaluated by the readers based on two criteria. First, overall image quality was scored based on a 5-point scale (1 = non-diagnostic images; 2 = poor quality and limited interpretation; 3 = moderate quality adequate for interpretation; 4 = good quality, permitting identification of fine anatomic structures and 5 = excellent quality, allowing definition of fine anatomic structures). Second, integer rank scores (-1 = worst; 0 = tie; 1 = best) were assigned to show the preference between two images in a pair. Wilcoxon signed-rank tests were used to analyze the image quality scores and image rank scores assigned by the two readers, with  $P < 0.05$  considered as statistically significant (27).

## Results

Bloch simulations show that the proposed preparation sequence achieves excellent suppression of the volume outside a 12 cm  $\times$  16 cm elliptical passband (Fig. 3 (a)). With a 20-ms  $T_2$  Prep time,  $B_1$  scale = 1 and spins on-resonance, the average  $M_z/M_0$  of arterial blood, myocardium and fat in the passband was 0.89, 0.62 and 0.02, respectively; while  $M_z/M_0$  in the stopband was below 0.07 for all three tissues. Figure 3 (b)–(d) demonstrates the performance across  $B_0$  and  $B_1$  variations within an off-resonance range of [-100, +100] Hz and  $B_1$  scale range of [80%, 120%]. Within this range of  $B_0$  and  $B_1$  variations, the  $M_z/M_0$  of arterial blood is  $0.88 \pm 0.02$  in the passband and  $0.08 \pm 0.05$  in the stopband; the  $M_z/M_0$  of myocardium is  $0.61 \pm 0.02$  and  $0.07 \pm 0.04$  in the passband and stopband, respectively.

Figure 4 summarizes the results of the phantom studies. The suppression outside the elliptical passband and  $T_2$  weighting inside the passband are well appreciated in the comparison between the images obtained with and without the preparation (Fig. 4 (a)–(b)). The quantitative ROI analysis shows that the normalized signal intensities of all four

phantoms are below 9% in the stopband (solid square) and agree well with the  $T_2$  exponential relationship in the passband (open circle vs. cross, absolute error  $< 0.06M_0$ ).

Figure 5 shows representative thin-slab MIP images from the in vivo coronary MRA scans with the full-FOV trajectory (FOV-28-Cones). The OVS- $T_2$  Prep sequence substantially reduced the outer volume signals while preserving the inner volume signals (Fig. 5 (a) vs. (d)) with improved blood-myocardium contrast (Fig. 5 (b)–(c) vs. (e)–(f)). Figure 6 displays examples of MIP images obtained with the FOV-16-Cones (acceleration factor of 1.8). Aliasing artifacts are observed in the RCA image obtained without preparation (arrow in Fig. 6 (a)), but are reduced in the images obtained with preparation (Fig. 6 (e)). With OVS- $T_2$  Prep, the depiction of the coronary arteries is improved and less aliasing is seen in the ventricles (Fig. 6 (b)–(d) vs. (f)–(h)). When the acceleration factor is increased to 3.5 with a scan time less than 3 minutes (FOV-8-Cones), the improvement with OVS- $T_2$  Prep is more noticeable (Fig. 7). Without OVS- $T_2$  Prep, the spatial aliasing degrades the image quality (Fig. 7 (a)–(d)). With OVS- $T_2$  Prep, the depiction of the LAD and RCA are improved due to the suppression of aliasing and enhanced blood-myocardium contrast (Fig. 7 (e)–(h)).

The quantitative analysis of full-FOV images yielded a passband-to-stopband signal ratio of  $3.18 \pm 0.77$  ( $R_{PS}$ ), and a significant increase in the blood-to-myocardium CNR ( $P < 0.001$ ) by a factor of  $1.43 \pm 0.20$  ( $R_C$ ). In the reduced-FOV images, the background signal ( $S_{BKGD}$ ) was reduced from  $7.13 \pm 1.25$  (without preparation) to  $4.72 \pm 1.16$  (with preparation) for FOV-8-Cones ( $P < 0.0001$ ) and reduced from  $4.63 \pm 0.96$  (without preparation) to  $3.11 \pm 0.68$  (with preparation) for FOV-16-Cones ( $P < 0.0001$ ), implying significantly less aliasing artifacts in both undersampled cones designs (Fig. 8).

The overall image quality score was significantly higher with OVS- $T_2$  Prep, for both FOV-8-Cones and FOV-28-Cones ( $P < 0.001$ ) (Fig. 9 (a)–(b)). The mean image quality score was improved with the preparation by at least 0.7 for all tested coronary locations and imaging FOVs. In comparison between FOV-8-Cones and FOV-28-Cones with preparation, the LAD image quality scores were not significant different ( $P = 0.807$ ); the difference in RCA scores was statistically significant but with a  $P$ -value close to the significance level ( $P = 0.047$ ). In the FOV-8-Cones case, the images obtained with preparation received higher rank scores in all the 26 LAD comparisons (13 pairs  $\times$  2 readers) and 22 out of 26 RCA comparisons (Fig. 9 (c)). In the FOV-28-Cones case, the images obtained with preparation received higher rank scores in 19 out of 26 LAD comparisons and 20 out of 26 RCA comparisons (Fig. 9 (d)). The rank scores with preparation were significantly higher than without preparation for both cones designs ( $P < 0.001$ ).

## Discussion

We have presented a magnetization preparation sequence that compactly combines OVS and  $T_2$  preparation, and its application for reduced-FOV coronary MRA. The simultaneous realization of OVS and  $T_2$  preparation by the proposed sequence has advantages over simple sequential application of the two preparations. First, the proposed OVS- $T_2$  Prep achieves zero delay between both preparations and the data acquisition, generating the combined

image contrast more accurately. Secondly, the OVS- $T_2$  Prep reduces the total number of RF pulses required, and therefore reduces the specific absorption rate.

A recent study also proposed coronary MRA with a combined OVS and  $T_2$  preparation pulse, in which a 2D spiral pulse is applied first as the tipdown pulse and then followed by a non-selective non-adiabatic tipup pulse (28). The two studies have their own merits in terms of the robustness to  $B_0$  and  $B_1$  inhomogeneities and scan time. While the approach in the present study achieves better stopband suppression with  $B_1$  variation because of the utilization of adiabatic BIR-4 pulse, the design in (28) preserves the passband signal better because the tipdown angle and tipup angle are consistent when  $B_1$  variation exists. Our work also used a significantly shorter spiral tipup pulse by utilizing the interleaved imaginary and real spatial profile of 2D spiral pulses (14). The short duration avoids potential blurring of the 2D tipup profile caused by field inhomogeneity. A potential issue with our sequence would be that tissues in the stopband experience  $T_1$  recovery during the  $T_2$  Prep time. This effect is alleviated with the two inversion refocusing pulses (22), which are able to suppress  $T_1$  species ranging from 200 ms to 1000 ms for  $T_2$  Prep times up to 100 ms (based on the criterion that average  $M_z$  over the stopband is less than  $0.1M_0$  in the presence of  $B_0$  inhomogeneity of  $[-100, +100]$  Hz and  $B_1$  variation of  $[80\%, 120\%]$ ). The use of cones trajectories allows for significant scan time acceleration and benign aliasing artifacts of diffuse pattern compared to the Cartesian readout. However, robust suppression of fat is challenging because of fat's rapid  $T_1$  recovery during the repeated acquisition of the k-space origin with cones. Although we used ATR-SSFP readout for further fat suppression, the sequence remains sensitive to large field inhomogeneity, which may cause aliasing artifacts in reduced-FOV images.

In addition to the capability of reduced-FOV imaging, another potential benefit of OVS- $T_2$  Prep is reduced respiratory motion artifacts. In free-breathing coronary MRA with retrospective motion correction, rigid-body motion correction methods are typically performed on the whole image volume to correct for global motion of the heart (29). However, these global correction techniques can introduce motion inconsistency artifacts because other structures such as the chest wall and spine move differently than the bulk cardiac motion. The OVS- $T_2$  Prep sequence suppresses signals from the structures outside the heart and may therefore reduce the motion inconsistency artifacts. This effect could be best assessed in the full-FOV studies that are free from the aliasing artifacts. Indeed, we observed improvements in image quality in several full-FOV images (e.g., Fig. 5 (b) vs. (e)), and significantly higher image quality scores and rank scores for the FOV-28-Cones RCA images with preparation than the images acquired without preparation. Likewise, in the reduced-FOV studies, it is possible that not only the suppressed aliasing of the outer volume, but also the improved motion correction contributed to the reduction of image artifacts.

In the rank analysis, none of the 52 image pairs resulted in lower rank scores from both readers for the images obtained with OVS- $T_2$  Prep. In six cases, the OVS- $T_2$  Prep images received lower rank scores from one of the two readers. Two of these six cases involved irregular breathing patterns that adversely affected image quality for both images, as reflected by image quality scores of 1 or 2. In the other four cases, both images scored with similarly high image quality (image quality scores of 3 or 4).

The proposed OVS- $T_2$  Prep sequence involves flexibility in its implementation and utilities. Although a fixed cylindrical passband was used in this study, the long and short axes of the in-plane passband can be re-sized on the y by scaling the X and Y spiral gradients independently for each subject. Reduced-FOV imaging with OVS- $T_2$  Prep can also be useful for high-resolution coronary MRA. A recent study demonstrated the feasibility of isotropic 0.8 mm-resolution coronary MRA using cones parallel imaging with an acceleration factor of 2.9 (30). By reducing the FOV with OVS- $T_2$  Prep, one can decrease the required acceleration factor and therefore reduce the SNR penalty. While tested at 1.5 T in this study, the OVS- $T_2$  Prep has a potential for 3 T, owing to the robustness to  $B_1$  inhomogeneities of the BIR-4 and AFP pulses. Although the 2D spiral tipup pulse is not adiabatic, the influence of an imperfect tipup angle on  $M_Z$  appears to be small (less than 5% error with  $\pm 20\%$   $B_1$  variation).

## Conclusion

We have presented a new magnetization preparation sequence for coronary MRA that simultaneously achieves OVS and  $T_2$  preparation with robustness to  $B_0$  and  $B_1$  inhomogeneities at 1.5 T. The proposed preparation sequence can substantially suppress the signal outside an elliptic cylinder passband while generating  $T_2$  contrast inside the passband, as demonstrated by phantom experiments and in vivo coronary MRA using full-FOV cones trajectories. In vivo studies using reduced-FOV cones trajectories showed that the proposed sequence significantly reduced aliasing artifacts as supported by reduced background signal intensity, enabling accelerated whole-heart coronary MRA in a scan time of less than 3 minutes.

## Acknowledgments

This work was supported by NIH, GE Healthcare.

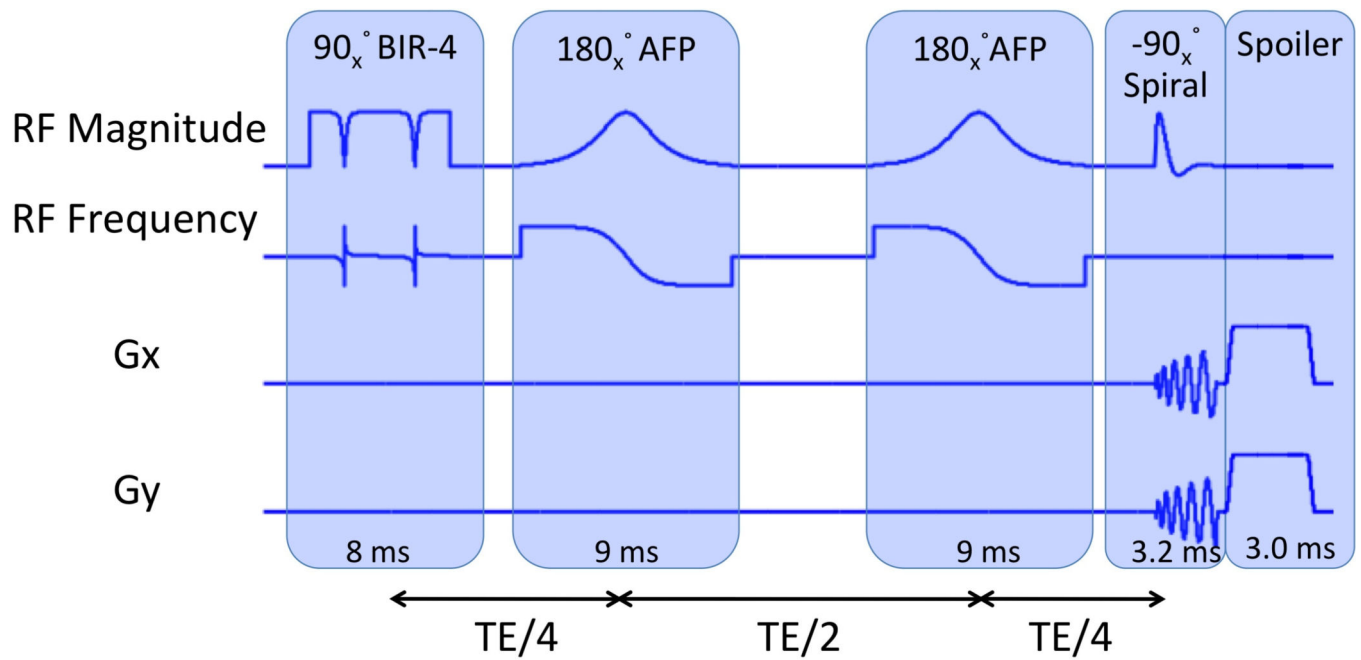
## References

1. Kato S, Kitagawa K, Ishida N, Ishida M, Nagata M, Ichikawa Y, Katahira K, Matsumoto Y, Seo K, Ochiai R, Kobayashi Y, Sakuma H. Assessment of coronary artery disease using magnetic resonance coronary angiography: A national multicenter trial. *Journal of the American College of Cardiology*. 2010; 56:983–991. [PubMed: 20828652]
2. Yang Q, Li K, Sun B, Yun H, Tang L, Li S, Cao Z, Xu J, Wei M, Jin L. Assessment of coronary artery disease using 3.0T magnetic resonance coronary angiography: a national multicenter trial. *Journal of Cardiovascular Magnetic Resonance*. 2013; 15(Suppl 1):E5.
3. Nagata M, Kato S, Kitagawa K, Ishida N, Nakajima H, Nakamori S, Ishida M, Miyahara M, Ito M, Sakuma H. Diagnostic accuracy of 1.5-T unenhanced whole-heart coronary MR angiography performed with 32-channel cardiac coils: Initial single-center experience. *Radiology*. 2011; 259:384–392. [PubMed: 21406635]
4. Niendorf T, Hardy CJ, Giaquinto RO, Gross P, Cline HE, Zhu Y, Kenwood G, Cohen S, Grant AK, Joshi S, Rofsky NM, Sodickson DK. Toward single breath-hold whole-heart coverage coronary MRA using highly accelerated parallel imaging with a 32-channel MR system. *Magnetic Resonance in Medicine*. 2006; 56:167–176. [PubMed: 16755538]
5. Akçakaya M, Basha TA, Chan RH, Manning WJ, Nezafat R. Accelerated isotropic sub-millimeter whole-heart coronary MRI: Compressed sensing versus parallel imaging. *Magnetic Resonance in Medicine*. 2014; 71:815–822. [PubMed: 23440946]

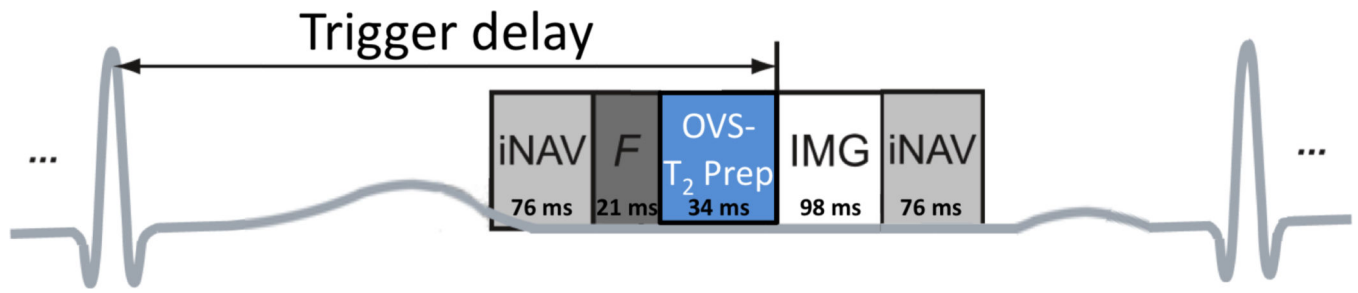


6. Akçakaya M, Basha TA, Chan RH, Rayatzadeh H, Kissinger KV, Goddu B, Goepfert LA, Manning WJ, Nezafat R. Accelerated contrast-enhanced whole-heart coronary MRI using low-dimensional-structure self-learning and thresholding. *Magnetic Resonance in Medicine*. 2012; 67:1434–1443. [PubMed: 22392654]
7. Meyer CH, Hu BS, Nishimura DG, Macovski A. Fast spiral coronary artery imaging. *Magnetic Resonance in Medicine*. 1992; 28:202–213. [PubMed: 1461123]
8. Salerno M, Sica CT, Kramer CM, Meyer CH. Optimization of spiral-based pulse sequences for first-pass myocardial perfusion imaging. *Magnetic Resonance in Medicine*. 2011; 65:1602–1610. [PubMed: 21590802]
9. Wu HH, Gurney PT, Hu BS, Nishimura DG, McConnell MV. Free-breathing multiphase whole-heart coronary MR angiography using image-based navigators and three-dimensional cones imaging. *Magnetic Resonance in Medicine*. 2013; 69:1083–1093. [PubMed: 22648856]
10. Ingle RR, Wu HH, Addy NO, Cheng JY, Yang PC, Hu BS, Nishimura DG. Nonrigid autofocus motion correction for coronary MR angiography with a 3D cones trajectory. *Magnetic Resonance in Medicine*. 2013
11. Le Roux P, Gilles RJ, McKinnon GC, Carlier PG. Optimized outer volume suppression for single-shot fast spin-echo cardiac imaging. *Journal of Magnetic Resonance Imaging*. 1998; 8:1022–1032. [PubMed: 9786138]
12. Schaeffter T, Rasche V, Brnert P, Mens G. Interactive reduced FOV imaging for projection reconstruction and spiral acquisition. *Magnetic Resonance Imaging*. 2001; 19:677–684. [PubMed: 11672626]
13. Pisani L, Bammer R, Glover G. Restricted field of view magnetic resonance imaging of a dynamic time series. *Magnetic Resonance in Medicine*. 2007; 57:297–307. [PubMed: 17260360]
14. Smith TB, Nayak KS. Reduced field of view MRI with rapid, B1-robust outer volume suppression. *Magnetic Resonance in Medicine*. 2012; 67:1316–1323. [PubMed: 22083545]
15. Brittain JH, Hu BS, Wright GA, Meyer CH, Macovski A, Nishimura DG. Coronary angiography with magnetization-prepared T2 contrast. *Magnetic Resonance in Medicine*. 1995; 33:689–696. [PubMed: 7596274]
16. Nezafat R, Stuber M, Ouwerkerk R, Gharib AM, Desai MY, Pettigrew RI. B1-insensitive T2 preparation for improved coronary magnetic resonance angiography at 3 T. *Magnetic Resonance in Medicine*. 2006; 55:858–864. [PubMed: 16538606]
17. Coristine AJ, van Heeswijk RB, Stuber M. Fat signal suppression for coronary MRA at 3T using a water-selective adiabatic T2-preparation technique. *Magnetic Resonance in Medicine*. 2013
18. Staewen RS, Johnson AJ, Ross BD, Parrish T, Merkle H, Garwood M. 3-D FLASH imaging using a single surface coil and a new adiabatic pulse, BIR-4. *Investigative Radiology*. 1990; 25:559–567. [PubMed: 2345088]
19. Ugurbil K, Garwood M, R RA, Bendall MR. Amplitude and frequency/phase modulated refocusing pulses that induce plane rotation even in the presence of inhomogeneous B1 fields. *Journal of Magnetic Resonance*. 1988; 78:472–497.
20. Silver MS, Joseph RI, Hoult DI. Highly selective  $\pi/2$  and  $\pi$  pulse generation. *Journal of Magnetic Resonance*. 1984; 59:347–351.
21. Conolly S, Nishimura D, Macovski A. Sweep-diagram analysis of selective adiabatic pulses. *Journal of Magnetic Resonance*. 1989; 83:549–564.
22. Dixon WT, Sardashti M, Castillo M, Stomp GP. Multiple inversion recovery reduces static tissue signal in angiograms. *Magnetic Resonance in Medicine*. 1991; 18:257–268. [PubMed: 2046511]
23. Leupold J, Hennig J, Scheffler K. Alternating repetition time balanced steady state free precession. *Magnetic Resonance in Medicine*. 2006; 55:557–565. [PubMed: 16447171]
24. Carr, JC.; Carroll, TJ. *Magnetic Resonance Angiography: Principles and Applications*. Springer; 2012.
25. Larson P, Gurney P, Nishimura D. Anisotropic field-of-views in radial imaging. *Medical Imaging, IEEE Transactions on*. 2008; 27:47–57.
26. Shin T, Nielsen JF, Nayak K. Accelerating dynamic spiral MRI by algebraic reconstruction from undersampled k–t space. *Medical Imaging, IEEE Transactions on*. 2007; 26:917–924.
27. McDonald, J. *Handbook of Biological Statistics*. Sparky House Publishing; 2009.

28. Coristine AJ, van Heeswijk RB, Stuber M. Combined T2-preparation and two-dimensional pencil-beam inner volume selection. *Magnetic Resonance in Medicine*. 2014
29. Henningsson M, Koken P, Stehning C, Razavi R, Prieto C, Botnar RM. Whole-heart coronary MR angiography with 2D self-navigated image reconstruction. *Magnetic Resonance in Medicine*. 2012; 67:437–445. [PubMed: 21656563]
30. Addy, NO.; Ingle, RR.; Nishimura, DG.; Hu, BS. High resolution variable-density 3D cones coronary MRA. *Proceedings of the 22nd ISMRM; Milan, Italy*. 2014. p. 2506

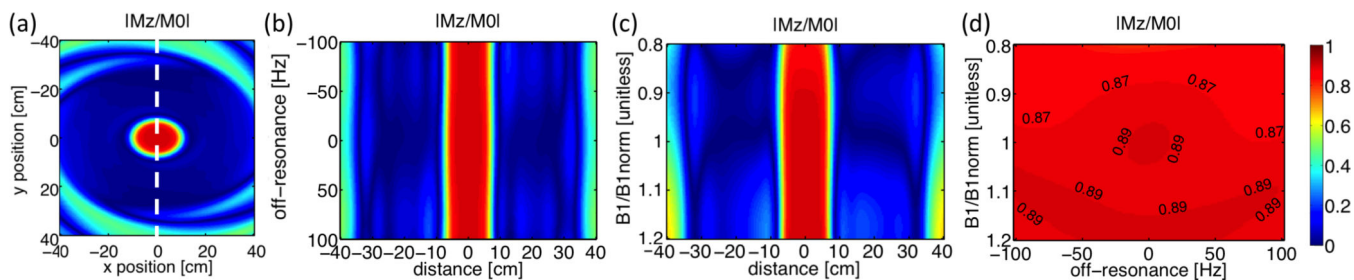


**Figure 1.** The timing diagram of the proposed OVS- $T_2$  Prep sequence, which consists of a  $90^\circ$  nonselective tipdown pulse (BIR-4:  $B_1$  insensitive rotation-4), two  $180^\circ$  refocusing pulses (AFP: adiabatic full passage pulses), a 2D spatially selective  $-90^\circ$  tipup pulse and spoiler gradients.



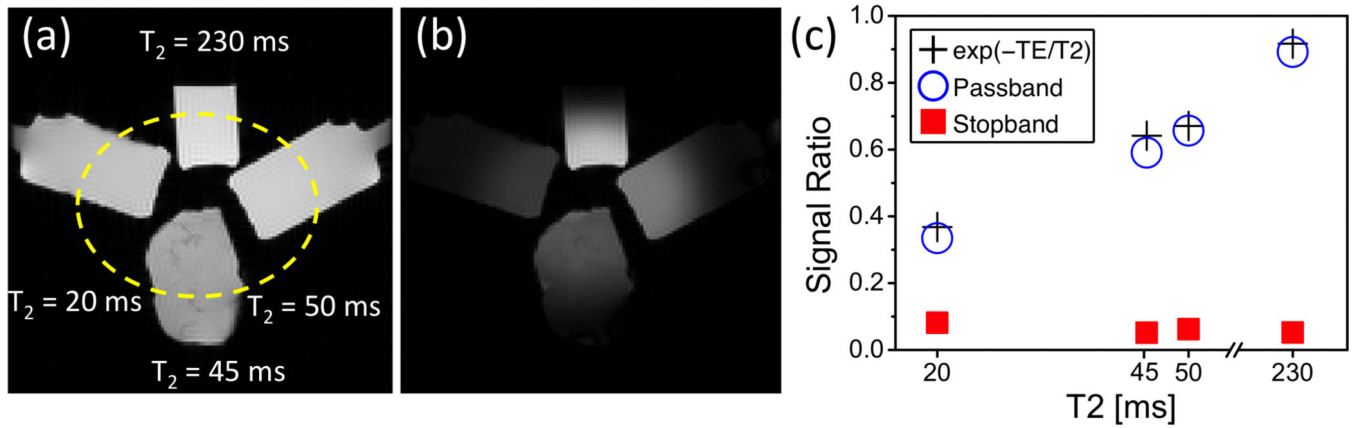
**Figure 2.**

The timing diagram of the free breathing coronary MRA sequence. iNAV: 2D spiral image-based navigators (76 ms). F: fat saturation (21 ms). OVS- $T_2$  Prep: proposed preparation sequence (34 ms). IMG: 3D cones image acquisition (98 ms).

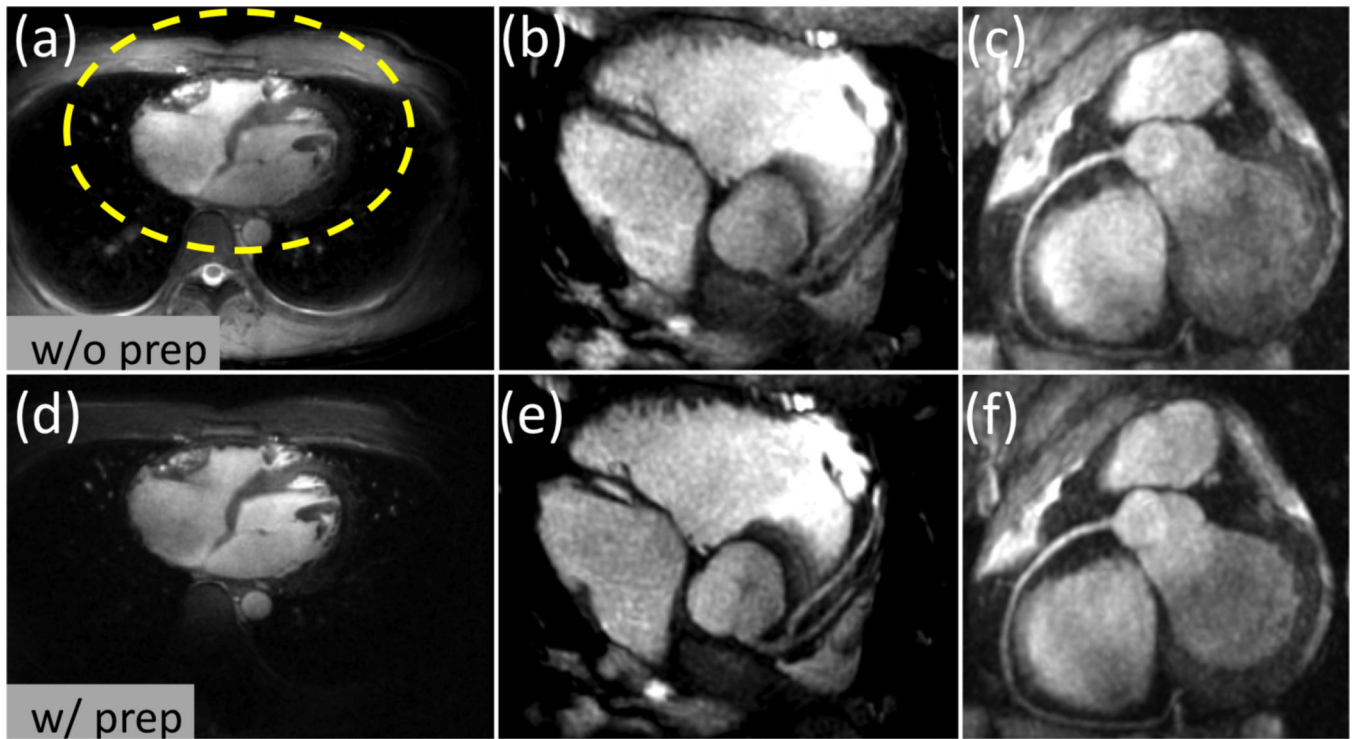


**Figure 3.**

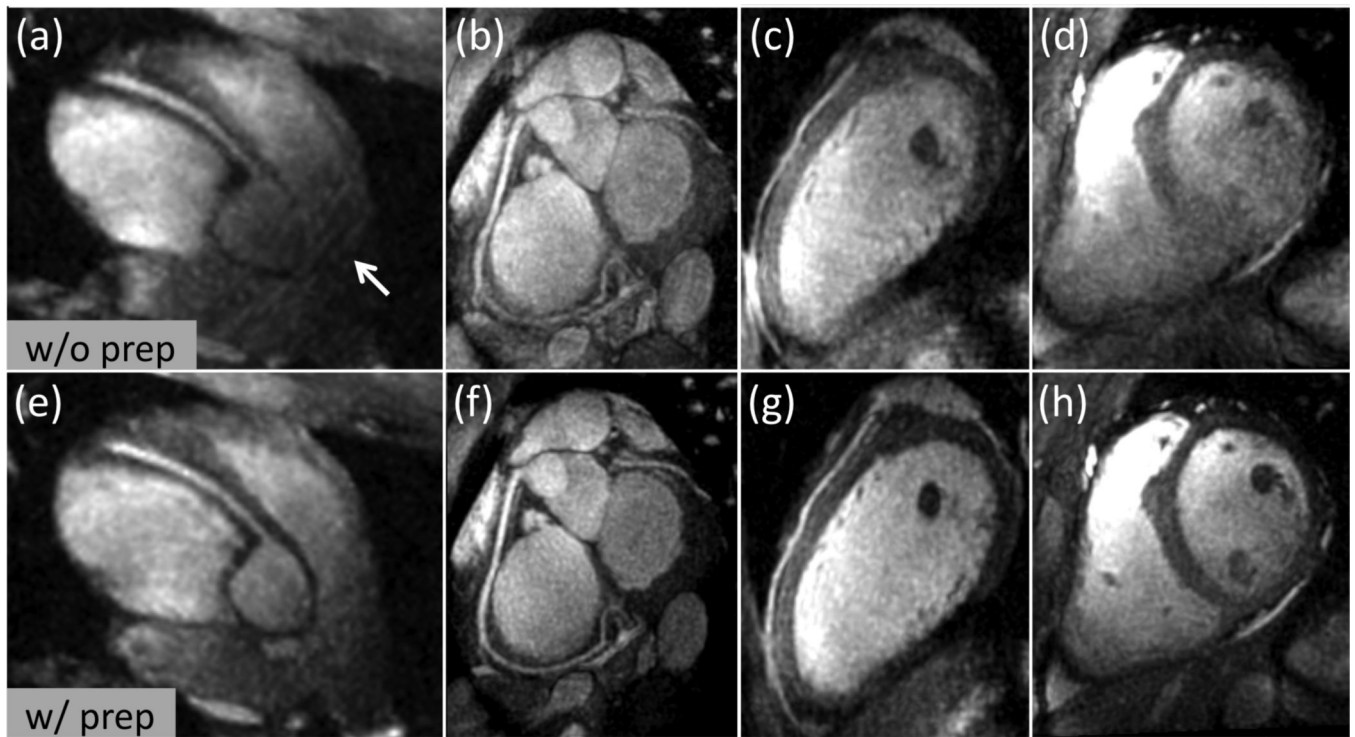
Bloch simulation results of OVS- $T_2$  Prep for arterial blood. (a): 2D distribution of resultant longitudinal magnetization on-resonance with  $B_1$  scale = 1. (b): Sensitivity to off-resonance with  $B_1$  scale = 1 at the short axis of the elliptical passband (dash line in (a)). (c): Sensitivity to  $B_1$  inhomogeneities on-resonance at the short axis of the elliptical passband (dash line in (a)). (d): Average longitudinal magnetization in the passband with  $B_0$  and  $B_1$  inhomogeneities.



**Figure 4.** OVS- $T_2$  Prep sequence performance in phantoms. Reference image obtained without preparation (a) and image obtained with OVS- $T_2$  Prep ( $T_2$  preparation time = 20 ms) (b) are shown with the same display window. (c): Ratios between the two images in ROIs in the passband (open circle) and the stopband (solid square). For all phantoms, the normalized passband signals agree well with the theoretical values (cross), while the normalized stopband signals are below 0.09.



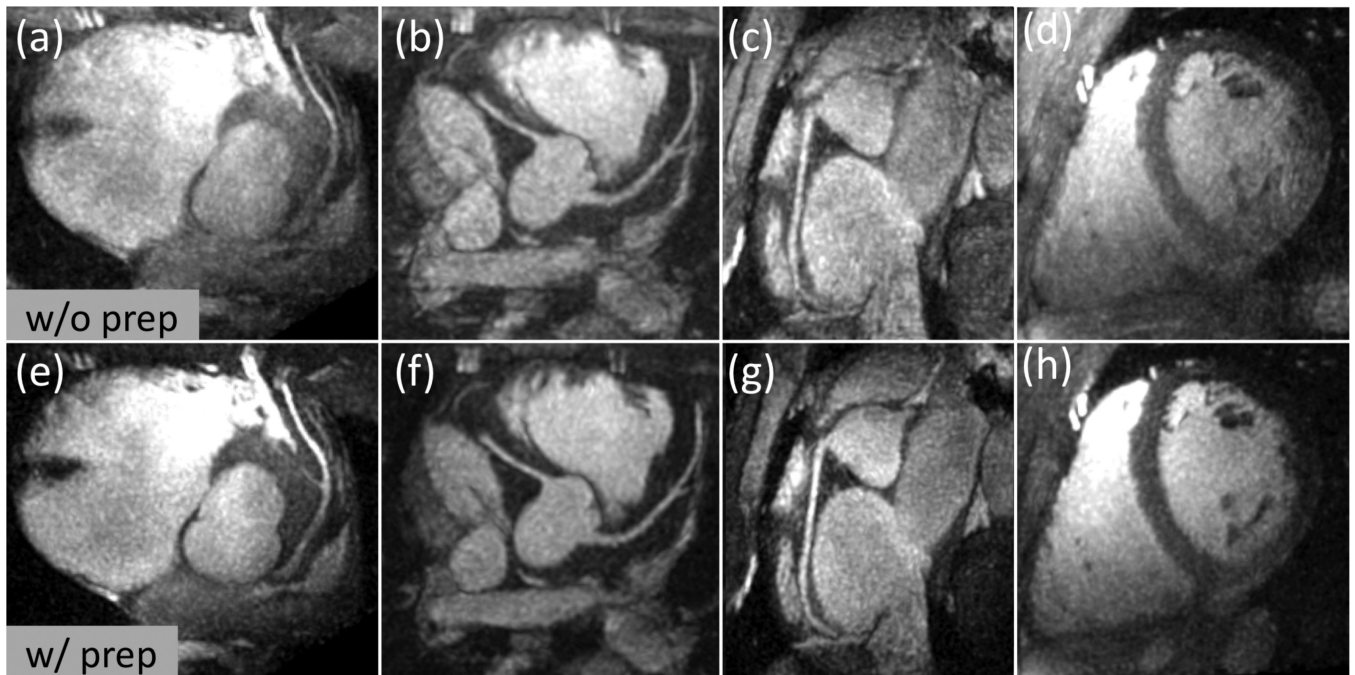
**Figure 5.** Representative thin-slab MIPs with FOV-28-Cones (acceleration factor 1) obtained without preparation (top row) and with preparation (bottom row). (a) and (d): Axial slice. (b) and (e): Reformatted view showing the LAD and LCx. (c) and (f): Reformatted view showing the RCA. The OVS- $T_2$  Prep substantially suppressed the signal outside the elliptical passband, and enhanced the blood-myocardium contrast.



**Figure 6.**

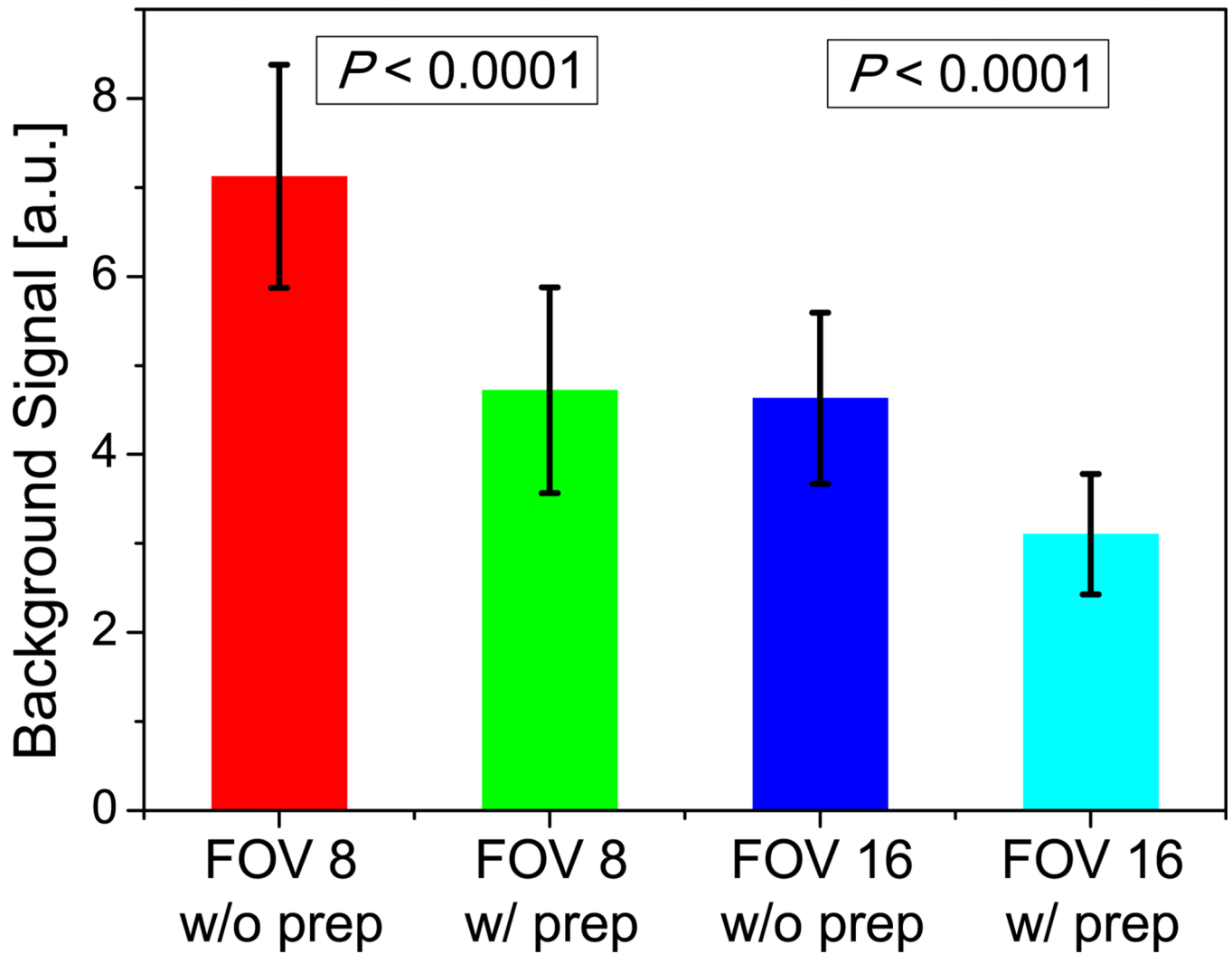
Representative thin-slab MIPs with FOV-16-Cones (acceleration factor 1.8) obtained without preparation (top row) and with preparation (bottom row). (a), (b), (e) and (f): Reformatted view showing the RCA. (c) and (g): Reformatted view showing the LAD. (d) and (h): Reformatted short axis view. Aliasing artifacts caused by k-space undersampling are observed in the images obtained without preparation (arrow), but are not noticeable in the images with the proposed OVS- $T_2$  Prep. Blood-myocardium contrast is also increased with the preparation.



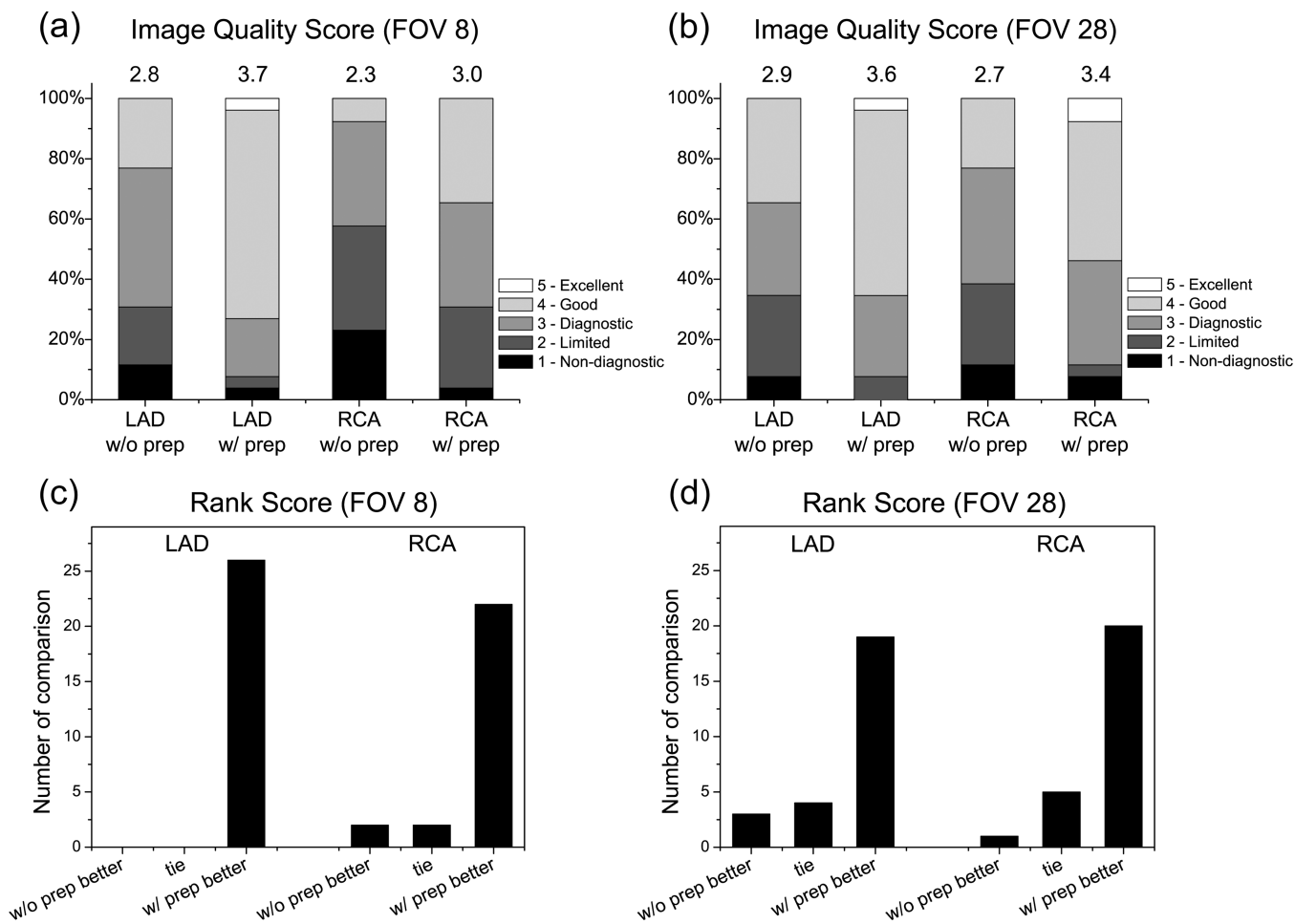


**Figure 7.**

Representative thin-slab MIPs with FOV-8-Cones (acceleration factor 3.5) obtained without preparation (top row) and with preparation (bottom row). (a) and (e): Reformatted view showing the LAD. (b) and (f): Reformatted view showing the left main, LAD and RCA. (c) and (g): Reformatted view showing the RCA. (d) and (h): Reformatted short axis view. Compared to the images obtained without preparation, the OVS- $T_2$  Prep reduced the aliasing artifacts, improving the depiction of coronary arteries and overall image quality.



**Figure 8.** Background signal as a quantitative metric for evaluating aliasing artifact. With preparation, the background signal is significantly lower for both FOV-8-Cones and FOV-16-Cones ( $P < 0.0001$ ).

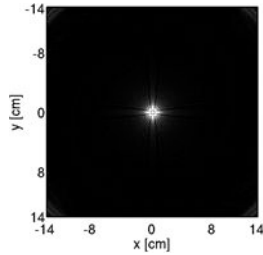
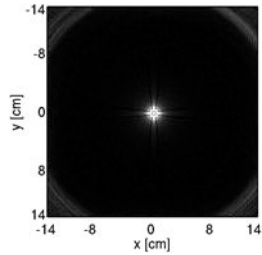
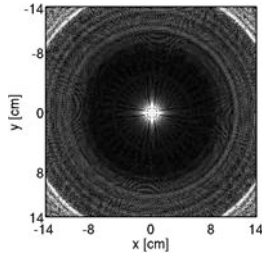


**Figure 9.**

Qualitative analysis of LAD and RCA obtained with and without OVS- $T_2$  Prep, using FOV-8-Cones and FOV-28-Cones respectively. (a) – (b) shows the image quality scores. Each color bar represents the percentage of number of the cases with the same score. The mean score is shown on top of the color bar. With preparation, the score of LAD and RCA were significantly higher than without preparation for both FOV-8-Cones and FOV-28-Cones ( $P < 0.001$ ). (c) – (d) shows the rank scores. The rank scores are represented as “w/o prep better” (image without preparation receives rank score 1), “tie” (both images receive rank score 0), “w/ prep better” (image with preparation receives rank score 1).

**Table 1**

Design Parameters of the Cones Trajectories for the In Vivo Studies

|  | FOV-28-Cones  | FOV-16-Cones   | FOV-8-Cones   |
|--|---|--|---|
| Design FOV [cm <sup>3</sup> ]                                | 28×28×14  | 16×16×14   | 8×8×14  |
| Scan time (for heart rate of 70 bpm)                         | 7 min 15 s  | 4 min 8 s  | 2 min 4 s   |
| Number of readouts   | 9142  | 5190   | 2607  |
| Acceleration factor  | 1   | 1.8  | 3.5   |
| Point spread function (displayed with the same window level) |  |  |  |
| Resolution   | isotropic 1.2 mm  |  |   |